Sustainable Computing: Informatics and Systems 34 (2022) 100666

Contents lists available at ScienceDirect

Sustainable Computing: Informatics and Systems

journal homepage: www.elsevier.com/locate/suscom

Fly, Wake-up, Find: UAV-based Energy-efficient Localization for Distributed Sensor Nodes

Vlad Niculescu [a,*], Daniele Palossi [a,b], Michele Magno [a], Luca Benini [a,c]

[a] Department of Information Technology and Electrical Engineering, ETH Zürich, Zürich, Switzerland
[b] Dalle Molle Institute for Artificial Intelligence, USI-SUPSI, Lugano, Switzerland
[c] Department of Electrical, Electronic and Information Engineering, University of Bologna, Bologna, Italy

ARTICLE INFO

Keywords:
UAVs
Wireless sensors
Ultra-wideband
Wake-up radio
Localization
Energy-efficiency

ABSTRACT

A challenging application scenario in the field of industrial Unmanned Aerial Vehicles (UAVs) is the capability of a robot to find and query smart sensor nodes deployed at arbitrary locations in the mission area. This work explores the combination of different communication technologies, namely, Ultra-Wideband (UWB) and Wake-Up Radio (WUR), with a UAV that acts as a "ubiquitous local-host" of a Wireless Sensor Network (WSN). First, the UAV performs the localization of the sensor node via multiple UWB range measurements, and then it flies in its proximity to perform energy-efficient data acquisition. We propose an energy-efficient and accurate localization algorithm – based on multi-lateration – that is computationally inexpensive and robust to in-field noise. Aiming at minimizing the sensor node energy consumption, we also present a communication protocol that leverages WUR technology to minimize ON-time of the power-hungry UWB transceiver on the sensors. In-field experimental evaluation demonstrates that our approach achieves a sub-meter localization precision of the sensor nodes – i.e., down to 0.6 m – using only three range measurements, and runs in 4 ms on a low power microcontroller (ARM Cortex-M4F). Due to the presence of the WUR and the proposed lightweight algorithm, the entire localization-acquisition cycle requires only 31 mJ on the sensor node. The approach is suitable for several emerging Industrial Internet of Things application scenarios where a mobile vehicle needs to estimate the location of static objects without any precise knowledge of their position.

1. Introduction

In the last decade, Unmanned Aerial Vehicles (UAVs) have been used in many applications, such as aerial inspection, surveillance, ambient awareness, and industrial applications [1–3]. A recent trend is their adoption as intelligent and ubiquitous coordinators of industrial Wireless Sensor Networks (WSNs), relieving the need for expensive infrastructure. WSNs are widely used for many practical industrial applications, such as remote monitoring or parcel tracking in big warehouses [4–6]. Usually, industrial WSNs contain a large number of simple, cheap, and resource-constrained (e.g., battery-powered) wireless sensor nodes deployed in wide indoor environments, such as warehouses and industrial facilities [5,7]. Within a WSN, data are first collected in some local-host, which forwards the relevant information to a central infrastructure that can be geographically decoupled from the deployment area [8]. In this context, UAVs are envisioned as an alternative to traditional gateways to overcome their limitations in terms of bandwidth, range, energy consumption and the need for physical infrastructure [7,9].

A UAV can quickly fly to any location within the mission area and reach all the WSN's nodes. In most real-world scenarios, the UAV's mission is to gather and exchange information from a group of sensor nodes deployed in the mission area. Once the UAV is in the proximity of the sensor node, it can act as an "intelligent and ubiquitous" local-host [9] and perform short-distance and therefore low-power data exchange. This can turn, for example, into a much longer lifetime of battery-powered sensor nodes deployed in an Industry 4.0 or Internet-of-things scenario, making the node last for months/years [10]. Furthermore, the drone could also perform wireless power transfer to charge the sensor node. By coming very close to the node, the drone can avoid power transfer losses due to the distance between the two [10]. However, in many real application scenarios, this vision is challenged by the unknown location of the WSN's nodes [8,11]. This is the case, for example, in dangerous or inaccessible areas, where the precise deployment of nodes is not feasible, such as areas affected by nuclear radiation (e.g., areas near nuclear reactors) [12]. With the advance of Industry 4.0, WSNs play an increasingly important role within the context of the

* Corresponding author.
E-mail address: vladn@iis.ee.ethz.ch (V. Niculescu).

https://doi.org/10.1016/j.suscom.2022.100666
Received 14 July 2021; Received in revised form 30 September 2021; Accepted 1 January 2022
Available online 15 January 2022

Table 1
Comparison against other localization systems. The red and green entries represent a lower and a higher performance compared to our system, respectively. The entries in black represent a similar performance, if applicable.

Metric	[18]	[19]	[20]	[21]	[22]	[23]	Our work
Technology	UWB	WiFi	BLE	BLE	UWB	UWB	UWB/WUR
Mean error (empirical data)	1 m	N/A	0.8 m	1 m	0.4 m	N/A	0.6 m
Mean error (synthetic data)	N/A	10 m	N/A	N/A	N/A	0.12 m	N/A
# measurements	3	3	100	140	6	3	**3**
Infrastructure-free	yes	yes	no	no	no	**yes**	**yes**
In-field evaluation	yes	no	yes	yes	yes	no	**yes**
Closed-loop demonstration	no	no	N/A	N/A	N/A	no	**yes**
Focus on energy saving	no	no	no	yes	no	**yes**	**yes**

Industrial Internet of Things (IIoT) and industrial smart buildings [13]. Such buildings often use industrial working spaces based on modular environments (e.g., reconfigurable floors or walls). These can change their configuration every time a new workshop is set up, and therefore the position of the nodes has to be redetermined. Similarly, the sensor nodes' deployment can be affected by inaccurate positioning in the area due to errors or hard-to-access areas (e.g., near a blast furnace) [13].

A potential solution to localize sensor nodes whose position is not known a priori is adding localization modules to them. Accurate estimation, small form factor, indoor operation capabilities, and low price are the primary asset in localization system design, especially in robotics and industrial WSN applications. A popular solution for localization is by equipping the sensor nodes with GPS receivers. However, GPS receivers consume on the order of tens of mW when active, and require around 30 s to acquire the first position measurement [14]. Unfortunately, this would dramatically increase the cost and power consumption of each sensor node, making the overall WSN lifetime constraint (e.g., the multi-year period between recharges) extremely difficult to meet. Techniques for reducing energy consumption, such as duty-cycling (i.e., enabling the GPS at a fixed period to obtain the position), have the disadvantage of introducing a high latency, which would result in long UAV mission times. Furthermore, GPS cannot operate in many industrial scenarios, where the GPS signal is blocked by the environment – i.e., GPS-denied areas –, and it is difficult to obtain sub-meter precision using absolute GPS positioning.

Ultra-Wideband (UWB) is an emerging technology enabling both distance estimation (ranging) and communication [15]. However, UWB has high power consumption when active (i.e., hundreds of mW). A viable option to overcome the UWB's high power consumption is to combine it with an ultra-low-power (i.e., a few μW) always-on receiver, such as Wake-Up Radio (WUR) technology [16,17]. WUR enables pure asynchronous communication that allows the sensor node to operate in sleep mode and wake up only when useful data transmission is required — e.g., when the UAV comes close. In this work, we pair UWB communication with WUR technology to achieve extremely energy-efficient localization of nodes in WSNs with a UAV acting as a mobile gateway. Due to the WUR, the UWB is only active for tens of ms during a localization cycle.

Multi-lateration is the heart of novel localization approaches based on UWB [24]. State-of-the-Art (SoA) localization solutions address the problem of localizing a moving object within the receptive field of, at least, three static UWB transceivers, called *anchors*. Although, in the context of large nodes' deployment areas, such as an industrial facility, this approach might lead to an unaffordable infrastructure cost and feasibility issues. Therefore, in our approach UWB is used to address the dual problem, i.e., the UAV acts as a "moving anchor" [18,24].

This paper proposes an energy-efficient localization system that combines UWB and WUR to enable UAVs to perform precise sensor node localization assuming Line-of-Sight (LOS) conditions for UWB communication. The paper presents an embedded multi-lateration algorithm that can run on any low power MCU. Specifically, our work provides the following contributions:

- an accurate flight policy paired with a lightweight multi-lateration algorithm, which guarantees an upper bound on the localization error of 0.6 m and runs in 4 ms on an ARM Cortex-M4 MCU, onboard our quadrotor;
- the combination of UWB and WUR technologies; the WUR enables the drone to perform "on-demand" wake-up, preventing the node from wasting energy in "always-on" or "duty-cycled" operation modes. A communication protocol orchestrates the interaction between our UAV (i.e., a quadrotor) and the sensor nodes. Thanks to the proposed protocol, the sensor node's energy consumption is ∼ 31 mJ for the whole localization and acquisition process;
- an in-field experimental evaluation of our UAV prototype, demonstrating its closed-loop functionality and a thorough analysis of the localization accuracy with in-field acquired UWB range measurements — i.e., affected by real-world noise.

Ultimately, our in-field evaluation shows that the proposed multi-lateration algorithm is up to 50 % more accurate than SoA, comparing it to similar "moving anchor-based" solutions [18].

The paper is structured as follows: Section 2 presents related works on UAVs, ranging technologies, and multi-lateration algorithms. Section 3 presents the theory behind our proposed multi-lateration algorithm and flight policy. Section 4 presents the hardware architecture and our communication protocol. Section 5 reports on experimental results, discussing and analyzing the main factors that influence localization accuracy and energy consumption. Section 6 discusses further factors (i.e., non-LOS conditions, range magnitude) which can impact the localization accuracy of our system. Finally, Section 7 concludes the paper.

2. Related work

Recent literature has shown an increasing interest in combining UAVs with WSNs for industrial applications, highlighting the reduction in cost/power compared to traditional long-range communications [9,11]. A common class of localization techniques employs range-based technologies [18,20,22], where the node's location is computed relative to multiple measurements from different spots visited by the UAV — i.e., way-points. The distance or angle (range information) between the drone and the node can be precisely measured using Received

Signal Strength Indicator (RSSI) [8], Time of Arrival (ToA) [24], Time Difference of Arrival (TDoA) [25], and Angle of Arrival (AoA) [26] techniques.

Wifi and Bluetooth are RSSI-based solutions, often mentioned as trendy choices due to their vast availability and reduced-price [8,27,28]. Bluetooth Low Energy (BLE) is a widely used technology in low power WSNs because it presents a reduced power consumption of a few tens of mW [29]. However, its precision when performing distance measurements is minimal and sensitive to noise. In [21], the proposed BLE-based localization scheme shows a minimum ranging error of about 1 m, which leads to a localization error of around 2 m, even in the optimistic case of more than a hundred measurements from seven fixed spots (i.e., anchors).

In contrast to these approaches, a novel ToA ranging method is represented by the UWB technology, which determines the range via the round trip time of the UWB signal, achieving centimeter accuracy in LOS conditions [24]. However, the ranging precision does not imply the same localization precision, which strongly depends on the relative position among way-points, noise on the ranging medium, and uncertainty in the UAV's self-localization — e.g., imprecise GPS coordinates. This paper proposes an energy-efficient and accurate localization system combining UWB and wake-up radio to detect battery-operated sensor nodes when their location is not precisely known.

Moving into the algorithmic navigation techniques based on ToA technology, *multi-lateration* is the most widely used due to its trade-off between computational requirements and localization accuracy, and we report a detailed comparison of the most relevant works [18–20,22] in Table 1. The table states the minimum mean error and its associated number of needed range measurements and the need for infrastructure, which indicates if the respective system works with fixed or mobile anchors. Furthermore, we evaluate if a localization system is tested with in-field acquired data and which solutions are deployed on a drone. Lastly, the table also compares energy-saving aspects for the sensor nodes, which is crucial for the WSN's lifetime.

The authors of [22] propose to use a cost function to penalize the localization error, but their approach requires a heavier memory footprint compared to our solution. Even if Table 1 indicates a smaller mean error associated with this work compared to our solution, their system uses six range measurements (and therefore more energy than ours), and it only works with an ad-hoc infrastructure — i.e., fixed anchors. [19] presents a localization algorithm that optimizes a cost function designed to minimize both the localization error and the energy consumed by a drone, but their approach has an inevitable accuracy drop due to the error/energy trade-off. The authors of [18] present a localization algorithm that bounds the localization error with a multi-lateration strategy similar to ours. Although, it requires a $\sim 40\,\%$ longer path (and flight time) to achieve the same accuracy of our approach. Furthermore, [30] presents a precise (up to 0.04 m accuracy in an ideal scenario) multi-lateration localization method called RB-MML, which is used in a wide range of localization systems [20] due to its reduced computational complexity given by its closed-form solution. However, this approach is mathematically developed assuming ideal conditions, and therefore it performs poorly in the presence of noise. In our previous work [31], we propose a solution for a drone looking for wireless sensor nodes exploiting UWB but only focusing on experiments with synthetic data. In this work, we extend our investigation by reproducing the experiments from [31] using empirical data. Moreover, we propose a flight policy for upper bounding the localization error and a communication protocol for achieving energy-efficiency for the node. Lastly, we perform an in-field evaluation of our prototype mounted on a commercial drone.

Even if the theoretical foundation of localizing sensor nodes with UAVs – i.e., moving anchors – has been addressed in several previous works [18,19], most of them report results based only on ideal synthetic data and/or lack of in-field deployment and demonstration. In contrast to them, we propose a lightweight algorithm that can run even in resource-constrained embedded platforms, achieving sub-meter localization accuracy in the presence of real-world effects, such as noise on the UWB range measurements and GPS localization inaccuracy. Moreover, our localization approach works with the minimum number of three range measurements, reducing flight time and the energy cost for the UWB communication. Lastly, due to the proposed WUR-based approach and the communication protocol, the energy consumption on each sensor node is minimized to a few tens of mJ, which leads to a power consumption of only 3.9 µW when the node is waiting for a new localization-acquisition cycle.

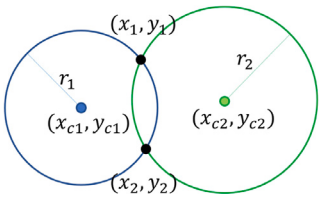

Fig. 1. Geometrical representation of two way-points.

3. The localization methodology

One of the main contributions of the paper is proposing an energy-efficient and accurate approach enabling UAVs to find wireless sensor nodes randomly deployed in the mission area. Thus, the paper focuses on a 2-dimensional (2D) use case, where all sensor nodes are deployed on the ground at the same altitude level. However, many key aspects of the proposed 2D use case also apply to the 3D case. Moreover, the 2D use case is still representative of most practical application scenarios [18,20] with WSNs.

3.1. Background: UWB multi-lateration

The purpose of a multi-lateration algorithm is to estimate the position of a not-localized static object on the ground – the sensor node in our case – with high accuracy, using way-points as input. A way-point is a structure of type (x_d, y_d, r), where the pair (x_d, y_d) represents the drone position (e.g., GPS position) [18], and r is the range measurement from the drone to the node (i.e., ground projection in a 2-D plane). Apart from the ranging error, the drone's GPS position and altitude measurements are also affected by noise, which consequently influences the accuracy of the multi-lateration estimation. More way-points lead to a more accurate estimation but also increases both the mission time, with more spots to be visited, and the number of transmitted packets, therefore increasing the energy consumption.

A common solution for fast multi-lateration is the RB-MML [30], which is used in a wide range of localization systems [8,27] due to its advantage of having a closed-form solution. Considering a noise-free scenario, the coordinates of the node and the N acquired way-points (x_i, y_i, r_i), with $i = 1, 2, \ldots, N$, satisfy Eq. (1).

$$(x_i - x)^2 + (y_i - y)^2 = r_i^2 \tag{1}$$

By subtracting the Nth equation from the first $N-1$ equations, results in a linear system of $N-1$ equations as the quadratic terms in x and y are canceled out, and the system can be solved in the least-squares sense. If the range distance measurements are not affected by any noise, RB-MML, as well as all other methods, provides the optimal node position using only three way-points. Computing the solution of RB-MML requires a few simple matrix multiplications, but when used in field applications, its accuracy drops quickly due to the inevitable measurement noise, as shown in Section 5.

Assuming that the noise that affects the range measurements is Gaussian with zero-mean, the maximum likelihood estimate is obtained by minimizing the cost function in Eq. (2) [22]. Therefore, the optimal

solution which minimizes the cost function is the pair $(\tilde{x}, \tilde{y})$ that makes the range measurements "the most likely". Our optimization problem is represented by the non-convex and non-linear function in Eq. (3). To avoid local minima, it is crucial to choose proper initialization values for (x, y), otherwise, the final solution might lead to high-cost values.

$$L(x,y) = \sum_{i=1}^{N} (\sqrt{(x_i - x)^2 + (y_i - y)^2} - r_i)^2 \tag{2}$$

$$(\tilde{x}, \tilde{y}) = \arg\min L(x,y) \tag{3}$$

3.2. Embedded multi-lateration algorithm

In the 2D case, the geometrical interpretation of a single way-point (x_1, y_1, r_1), suggests that the sensor node is somewhere on the circumference of the circle with center in (x_1, y_1) and radius r_1. With a second way-point, the number of possible locations for the node is reduced to two possibilities: the two points given by the intersection of the two circumferences, as shown in Fig. 1. We note as $\mathbf{C_1}$ the circle of radius r_1 and center in (x_{c1}, y_{c1}) and as $\mathbf{C_2}$ the circle of radius r_2 and center in (x_{c2}, y_{c2}). The intersection points of the two circles (x_1, y_1) and (x_2, y_2) can be easily computed using the equations in [32]. The proposed approach computes the cost function in Eq. (2) for both the two candidate points, considering all the N way-points, and we select as (x_0, y_0) the one which leads to the smaller cost.

Algorithm 1 Gradient descent with adaptive learning rate. $\mathbf{C_1}$ and $\mathbf{C_2}$ are the two circles depicted in Fig. 1, whose intersection gives the two candidate points for initializing the gradient descent.

(x_1, y_1) and $(x_2, y_2) \leftarrow \mathbf{C_1} \cap \mathbf{C_2}$;
$L_1 = L(x_1, y_1)$;
$L_2 = L(x_2, y_2)$;
if $L_1 < L_2$ **then**
  $(x_0, y_0) = (x_1, y_1)$;
else
  $(x_0, y_0) = (x_2, y_2)$;
end
$x = x_0$;
$y = y_0$;
$iterations = 0$;
while *(iterations <20)* **do**
  $iterations \leftarrow iterations + 1$;
  $H_{L(x,y)} \leftarrow \begin{bmatrix} \frac{\partial^2}{\partial x^2} L(x,y) & \frac{\partial^2}{\partial x \partial y} L(x,y) \\ \frac{\partial^2}{\partial y \partial x} L(x,y) & \frac{\partial^2}{\partial y^2} L(x,y) \end{bmatrix}$;
  $\begin{bmatrix} \alpha_1 \\ \alpha_2 \end{bmatrix} \leftarrow [H_{L(x,y)}]^{-1} \begin{bmatrix} \frac{\partial}{\partial x} L(x,y) \\ \frac{\partial}{\partial y} L(x,y) \end{bmatrix}$;
  $x \leftarrow x - \alpha_1 \frac{\partial}{\partial x} L(x,y)$;
  $y \leftarrow y - \alpha_2 \frac{\partial}{\partial y} L(x,y)$;
end

In an ideal case, where the range measurements are not affected by any sensor noise, the solution (x_0, y_0) represents the global minimum of the optimization problem given by Eq. (3) and leads to a cost equal to zero. However, in practice, range measurements are never noise-free, and the noise standard deviation impacts how far (x_0, y_0) is with respect to the global minimum of the optimization problem. Nevertheless, range measurements have a precision of 10 cm, as they are acquired via UWB. Since the UWB distance measurements are in the range of meters, their cm error practically results in having the (x_0, y_0) solution located near to the global minimum. In our work, we do not provide any formal demonstration on the optimality of our multi-lateration algorithm for minimizing the cost function because this optimization problem is non-linear, non-convex, and can have several local minima. However, we use empirical evidence to prove that in practice, our approach converges to the global minimum. To determine the global minimum ground truth, we performed a grid search varying x and y with a step of 0.5 cm and chose the global minimum as the pair (x,y) that leads to the smallest cost. We ran 1000 experiments, and we observed that in all situations, the proposed algorithm initialization (x_0, y_0) is found in a convex vicinity of the global minimum, and with such an initialization, the algorithm finds the global minimum in every experiment. Consequently, we use (x_0, y_0) as the initialization value for the optimizer.

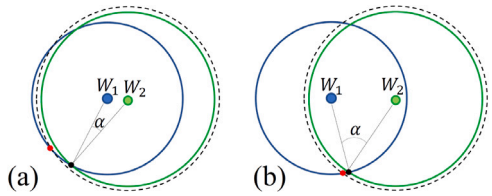

Fig. 2. Effect of noise (dashed circles) for small (a) and large (b) α angle leading to a wrong localization (red dots). (For interpretation of the references to color in this figure legend, the reader is referred to the web version of this article.)

The proposed optimization approach is a gradient descent algorithm meant to run in a low-resources embedded platform. To minimize the number of iterations until convergence, we use Newton's update rule to online adjust the learning rate of the algorithm with respect to the inverse of the Hessian matrix [33], as shown in Algorithm 1. With this choice, the optimizer converges faster in the first few iterations and the learning rate decreases as they progress (on average from 0.5 to 0.001). Experimentally, we observed that Algorithm 1 achieves a difference of less than 1 mm between two consecutive iterations after less than 20 iterations. In this way, our algorithm is not data-dependent, and the iteration number – and also running time – is always constant and predictable (4 ms for an ARM Cortex M4@168 MHz).

3.3. The flight policy

Recalling the geometrical representation from Fig. 1, we consider two other similar situations depicted in Fig. 2. In both sub-figures, the solid-line circles (blue and green) represent two noise-free range measurements, associated with two distinct way-points. However, in practice, both range measurements are affected by noise. Without loss of generality and only for the sake of this example, we can consider the case of only one of the two being corrupted by noise, as the dashed circle indicates in Fig. 2.

Comparing Fig. 2(a) with Fig. 2(b), it is clear that the higher the overlapping of the two areas defined by the two circles is, the higher the localization error is. This overlapping degree can be geometrically paired to the angle formed by the two way-points and the node position — called alpha (α). We point out that this example is only given to motivate that the locations where the range measurements are acquired have an impact on the node localization error, and this is why we only considered that one range measurement is noisy. However, everything applies also to the case of multiple noisy range measurements, as it is also considered in Section 5. Our flight policy aims to minimize the localization error, keeping the number of way-points low and, therefore, the number of range measurements.

To keep our flight policy as general as possible, we propose to use three equally spaced way-points, which involve the drone flying the shape of an equilateral triangle and acquire a range measurement in each vertex (A, B, and C), as Fig. 3(a) shows. Given the three way-points measurements and the sensor node position (N), we can always derive three angles with respect to N ($\widehat{ANB}$, $\widehat{BNC}$, and $\widehat{CNA}$). We call α_1 and α_2, the two smaller angles among the three for which no other way-point lies in between, as represented in Fig. 3(b). This policy leads us to three possible cases:

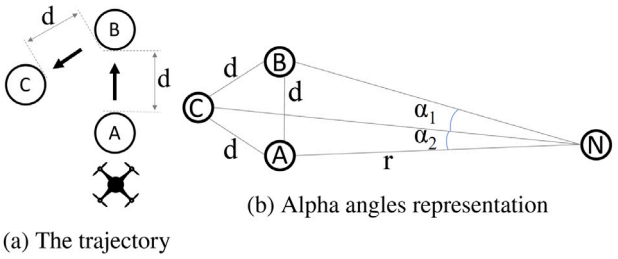

(a) The trajectory (b) Alpha angles representation

Fig. 3. (a) Sequence of way-points (A, B, and C) acquisition. (b) shows the node position (N) and the two α angles.

- N is inside or on the triangle;
- N is outside the triangle, and α_1 and α_2 are non-zero;
- N is outside the triangle and α_1 or α_2 is zero — i.e., two vertexes are collinear to N.

Since the localization error depends on the sum of α_1 and α_2, and increases as this sum decreases, as thoroughly analyzed in Section 5, the last case of collinear vertexes represents our worst-case, because it leads to the smallest sum. Therefore, bounding the localization error for this case will also bound the error for any possible alpha angle. When the drone acquires the first range measurement (r) in A, the only parameter which can be set before moving to the next locations (B and C) is the edge length of the triangle (d). In this worst-case, the relation between d, the non-zero α, and r is given by Eq. (4) which is used to bound the error, enforcing a minimum alpha angles sum (e.g., $\alpha_1 + \alpha_2$). As Eq. (4) represents the case of the sensor node (N) lying outside the triangle, it holds for sums of alpha angles smaller than 60°. Higher sums of alpha angles that would lead to a smaller localization error cannot be guaranteed a priori with our strategy, even if they can be obtained in practice during the mission. Thus, to have analytical guarantees on sub-meter errors (i.e., paired to $\geq 60°$ sum of angles), we would need a flight policy based on more than three way-points.

$$d = \frac{2r \sin\alpha(\sin\alpha + \sqrt{3}\cos\alpha)}{4\cos^2\alpha - 1} \tag{4}$$

4. System architecture

This section introduces the hardware design of the proposed system and the communication protocol. The combination of the two enables precise and energy-efficient interaction between a commercial quadrotor and the sensor nodes randomly deployed in the mission area.

4.1. Hardware design

To run our multi-lateration algorithm, we designed an add-on printed circuit board (PCB), called *localization unit* as shown in Fig. 5A, to be placed aboard a commercial standard-size drone. It manages the communication with the nodes, acquires the range measurements, performs the sensor node localization, and sends trajectory commands to the drone; therefore, it handles all the operations in closed-loop. The localization unit features an ARM Cortex M4 MCU, a GPS module uBlox M8T, a high precision barometer TE MS6511, a UWB module Decawave DWM1000, and a radio transceiver TI CC1200 . The GPS module is used only to determine the latitude and the longitude of the drone, while the barometer provides altitude information relative to the ground level, resulting in a complete 3-D position estimation of the drone. The 868 MHz onboard radio transceiver is used to emit wake-up beacons to wake up the sensor nodes deployed on the mission area.

Fig. 5B shows the designed and implemented wireless sensor node that is equipped with solar energy harvesting that continuously charges the battery of the sensor node. The sensor node features an STM32L433 MCU, the same UWB module used on the localization unit, a custom WUR module [16], and an energy harvesting subsystem, built around the TI BQ25570 converter — the harvester can extend the battery lifetime of the node, but in this work, we do not perform any analysis on the harvesting capabilities, since it is out of the scope of UWB-based sensor node localization. The MCU manages the sensor's data acquisition, and it is in charge of controlling the UWB module in the ranging process as well as its power mode. The UWB module uses a chip antenna[1] and it is configured for the maximum transmit power and the smallest data-rate (110 kbps) to maximize the operating range (up to 150 m LOS). It uses a center frequency of 3.99 GHz and a bandwidth of 500 MHz. The WUR module is responsible for waking up the MCU when a wake-up beacon is received from the localization unit and it features addressing capabilities to elicit the response by a single node of the WSN. The sensor node hosts the WUR designed from [16]. In our implementation, the WUR achieved a sensitivity of -55 dBm while listening for beacons, that in combination with the radio transceiver of our localization unit (TI CC1200) can cover a range up to 35 m using a −2.3 dBi[2] antenna and 14 dBm of output power. During the whole localization-acquisition cycle, the sensor node consumes a total energy of 31 mJ.

4.2. Communication protocol

The goal of the proposed asynchronous communication protocol is to exploit the WUR, achieving highly energy-efficient interaction during the localization-acquisition cycle between the localization unit and the sensor nodes. nodes. The protocol enables sequential localization, which means that the drone localizes one sensor node after the other. Because it is not possible to perform concurrent UWB ranging with addressing, overlapping UWB range measurements from multiple nodes would result in the same total localization time. Furthermore, in our application scenario, we use the addressing capabilities of the WUR to ensure that only one node is woken up at a time and responds to the drone for performing localization. The order in which the drone sends the wake-up messages, dictates which node would reply first, in a scenario where multiple nodes are located in the drone's vicinity. Fig. 4 describes, without loss of generality, the drone-nodes interaction for three way-points. It also highlights the power regime of each module on the sensor node — i.e., MCU (M), UWB (U), and WUR (W) black when active. Table 2 shows the sensor node's power consumption for the following main states:

Listening: All node's electronics are in the lowest power mode: *sleep mode*. The MCU's core and its peripherals are disabled, but when the WUR receives a wake-up radio beacon, the MCU is woken up via interrupt, entering the *ranging state*. When a wake-up beacon is sent by the localization unit only the addressed node is activated, leaving all the others inactive (in *listening state*). During this state the power consumption on the sensor node for the MCU, UWB and WUR modules are 0.2 µW, 1.4 µW, and 2.3 µW, respectively — total 3.9 µW as reported in Table 2.

Ranging: In this state, the node initiates the double-sided two-way ranging process sending a UWB message, waiting for a reply from the localization unit, and going back to the *listening state* in case of time-out on the reply message. During this state, the UWB module operates at its maximum power (400 mW peak) to achieve a high communication range. When the ranging process is complete, the localization unit obtains a distance measurement, the node enters the *waiting state*, and it waits either for a new iteration of the ranging acquisition or to perform the data transfer to the localization unit — i.e., *acquisition state*.

Waiting: After the drone acquires a range measurement, it calculates the distance to the next way-point using Eq. (4), and it flies

[1] https://datasheet.lcsc.com/szlcsc/Partron-ACS5200HFAUWB_C224424.pdf.

[2] http://linxtechnologies.com/wp/wp-content/uploads/ant-868-cw-hwr.pdf.

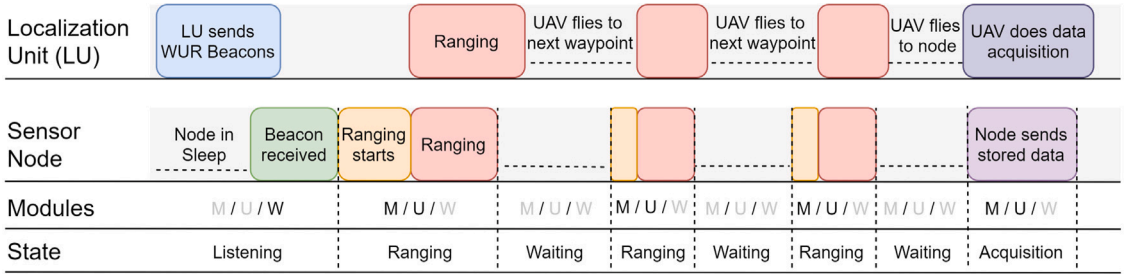

Fig. 4. The localization protocol. The labels MCU (M), UWB (U), and WUR (W) are marked with black when active.

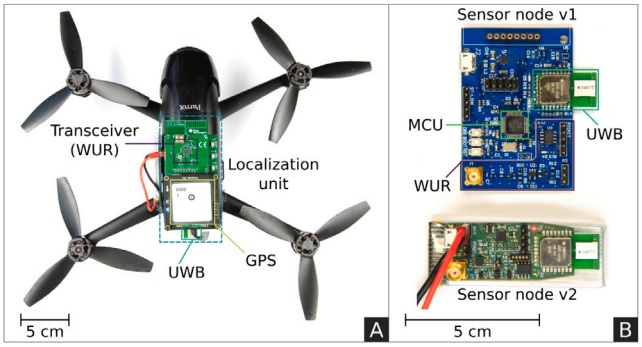

Fig. 5. (A) Our prototype is based on a commercial-of-the-shelf (COTS) Parrot Bebop 2 extended with our localization unit. (B) Sensor node, both v1 and v2 (optimized form factor).

Table 2
Sensor node power consumption (per state).

Listening	Ranging	Waiting	Acquisition
3.9 µW	300 mW	1.2 mW	300 mW

there to perform a new range acquisition. During this time, the node's MCU reduces its clock frequency to 100 kHz to save energy, and all other node's electronics go in *sleep mode*, keeping the memories in a persistent state, with a total power consumption of 1.2 µW. The sensor node iterates between *ranging state* and *waiting state* until the drone obtains all the expected range measurements (three in Fig. 4), in which case it enters the *acquisition state*.

Acquisition: Once the localization unit has obtained all the required range measurements, it runs the multi-lateration algorithm and flies above the localized node to acquire its data. During this flight, the node is in the *waiting state* to wake up once the drone has reached its position and starts the UWB data exchange. For the data transfer, the UWB is set to the highest data-rate (i.e., 6.8 Mbps) to reduce the transfer time and peaking at 300 mW of power consumption. Once the data acquisition is completed, the node goes back to the *listening state*.

5. Experimental results

This section presents the experimental results and analysis of the embedded multi-lateration algorithm presented in Section 3 and evaluated on the prototypes presented in the previous section. The evaluation is performed with three types of data: synthetic range measurements, real-world UWB measurements acquired on the ground, and real-world UWB measurements obtained with a flying drone. Our synthetic data are generated by altering the range measurements by zero-mean Gaussian noise ($\sigma_r = 10$ cm, according to the UWB module data-sheet), leaving the way-points location unaltered. The main difference between real-world UWB measurements acquired on the ground vs. a flying drone is the GPS positioning errors, not present in the former. Although, all real-world measurements are characterized by non-Gaussian noise

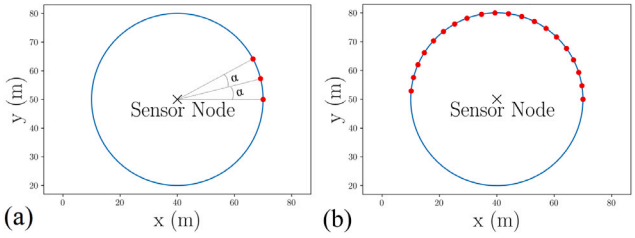

Fig. 6. The red spots indicate the location where the drone acquires a new way-point. (a) Alpha angle is varied. (b) Way-point density is varied.

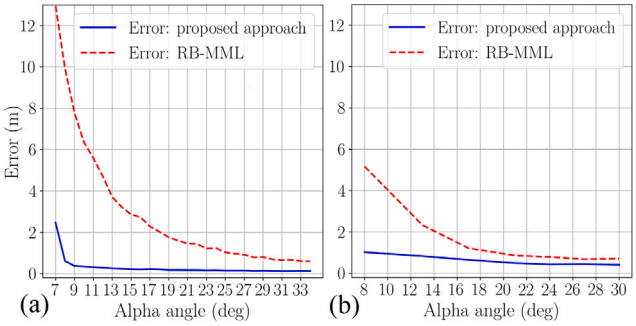

Fig. 7. Localization error as a function of alpha angle ($\alpha_1 = \alpha_2$), for the configuration shown in Fig. 6(a). (a) Synthetic data. (b) Real-world UWB measurements.

– in contrast with synthetic data – due to factors like Non-Line-of-Sight (NLOS) conditions or antenna delays, which can have a significant impact on the overall localization accuracy. Other works [34] show that the UWB error statistics (i.e., mean and variance) depends on the UWB antenna orientation and can reach values up to 0.4 m.

In the rest of this section, we refer to the way-point structure (x_d, y_d, r), where x_d and y_d are calculated by converting GPS latitude and longitude, into Cartesian coordinates (*east-north-up* coordinate system). The ground distance – i.e., the 3D projection on the ground of the UWB range measurement – is calculated as $r = \sqrt{z^2 - a^2}$, where z is the UWB range measurement, and a is the altitude (onboard barometer).

5.1. Localization accuracy with synthetic and ground data

In the first experiment described in Fig. 6(a), the node position is estimated via multi-lateration performing an acquisition procedure where the drone visits three different way-points on a circular trajectory, and it acquires a new measurement for each of them. The alpha angle (α) is represented as a central angle due to the selected trajectory, and we always enforce two equal alpha angles ($\alpha_1 = \alpha_2$) by selecting the visited way-points. A smaller alpha angle implies a shorter flying distance and a faster way-point acquisition, which is essential to minimize the overall drone's energy consumption.

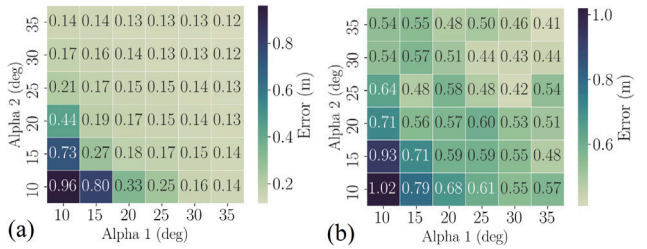

Fig. 8. Localization error as a function of the two alpha angles. (a) Synthetic data. (b) Real-world UWB measurements.

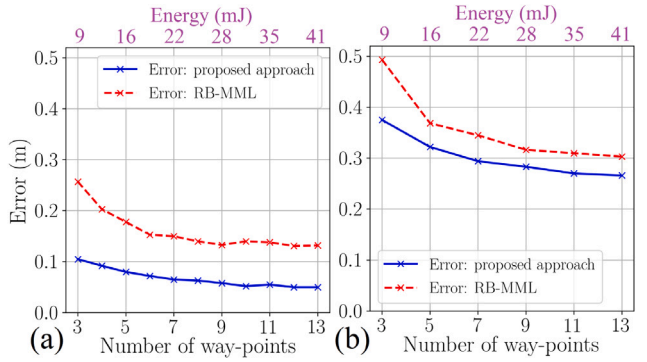

Fig. 9. Localization error as a function of way-point number and UWB energy consumption. (a) Synthetic data. (b) Real-world UWB measurements.

Fig. 7 shows the mean localization error, as a function of the alpha angles, both with synthetic data (Fig. 7(a)) and with real-world UWB measurements acquired on the ground (Fig. 7(b)). For the former experiment, the alpha angle is swept in the range 7°-34°, and between 8°-30° for the latter, with an incremental step of 2° for both of them. This localization error is evaluated for both the proposed approach and the RB-MML algorithm [30]. Results highlight how our approach outperforms the RB-MML baseline for both synthetic and real-world data. In Fig. 7(a), we have a reduction of $\sim$ 6× of the peak error (α = 7°) and minimum error for the proposed algorithm as low as 12 cm vs. 58 cm for RB-MML. In Fig. 7(b), we observe a reduction of $\sim$ 5× of the peak error (α = 8°) and minimum error for the proposed algorithm as low as 20 cm vs. 36 cm for RB-MML. For small alpha angle values, both algorithms seem to perform better on real-world data, since different antenna's orientations can lead to a UWB measurements standard deviation lower than 10 cm — as it is assumed for the synthetic data.

In Fig. 8, we present a second experiment based on the configuration shown in Fig. 6(a), but this time we explore the localization error trade-off of different alpha angles. The results for both synthetic and real-world data demonstrate how the localization error depends on the sum of both angles, and how it can be significantly reduced, increasing them. We can also observe that the error is equally dependent on both alpha angles, being almost constant along the main diagonal and its parallels (i.e., from top-left to bottom-right corner). Although, the results for the real-world UWB measurements show higher variance on all diagonals due to additional source of noise, like biases and/or antenna delays.

In Fig. 9, we report the mean localization error as a function of the number of way-points, considering them uniformly distributed on the semi-circumference of a circular trajectory, as shown in Fig. 6(b). Also, in this case, our proposed multi-lateration approach performs on average 2× better than RB-MML for synthetic data, and 20 % better on real-world UWB measurements. From Fig. 9, we can see how our approach improves increasing the number of way-points from 3 to 13, of 40 % and 30 %, using synthetic data (Fig. 9(a)) and real-world UWB measurements (Fig. 9(b)), respectively. Such an improvement comes at the price of increased UWB activity and flight time due to the additional range measurements to be acquired. Fig. 9 not only shows how the localization precision changes with the number of way-points, but also the total energy consumed by the node's UWB and, therefore, the trade-off between precision and energy. The sensor node's UWB energy consumption is proportional to the number of way-points, and it ranges between 9 mJ (3 way-points) and 41 mJ (13 way-points).

Table 3
Energy consumption as a function of the duty cycle and number of way-points (UWB and WUR only).

			Number of way-points		
			3	8	13
no WUR(UWB)	DC	1.5%	12969 mJ	12983 mJ	12997 mJ
		1%	8549 mJ	8663 mJ	8677 mJ
		0.5%	4329 mJ	4343 mJ	4357 mJ
WUR		–	17 mJ	31 mJ	46 mJ

In Table 3, we perform a quantitative two-dimensional analysis of the sensor node's energy consumption. In this experiment, the node waits in the *listening state* for one hour, and then the drone wakes it up to perform the localization and acquisition. The energy that we report in Table 3 represents the energy consumed by the UWB and WUR only. Along the horizontal direction, our results show the energy demands when the number of UWB range measurements increases. Furthermore, we also include a second dimension of exploration along the vertical direction. We present how the consumed energy increases when we use the UWB module instead of the WUR in the *listening state*. Due to the high power consumption during receiving, we use duty-cycling so that the UWB is periodically waking up to poll for a message from the drone, and then it goes back in the sleep mode. We choose a duty-cycle (DC) value of $1 \pm 0.5\%$, because this is a realistic value that would result in a latency of less than 1 s — higher latencies would limit unrealistically the flying speed of the drone. When using the WUR in the *listening state*, the energy consumption depends more on the number of way-points, because the WUR energy consumption (8 mJ) is smaller than the energy consumed by the UWB during ranging. On the other hand, for the scenarios that use UWB and duty-cycling in the *listening state*, the energy consumption is almost constant along the table lines due to the high energy consumption of the duty-cycled UWB. Table 3 shows that the most energy-efficient configuration (17 mJ) corresponds to three way-points with the WUR used for listening. In comparison, the highest energy consumption (12 997 mJ) corresponds to the other extreme of the secondary diagonal, which uses 13 way-points and a duty-cycle of 1.5%.

In the next experiment, we investigate the energy consumption for multiple configurations of the number of way-points, and the packet size exchanged during the *acquisition state*, the latter depending on the specific use-case. In this experiment, we assume the drone flying with an average speed of $3\,\mathrm{m\,s^{-1}}$ and a travel-distance between two consecutive way-points of 10 m. Fig. 10 shows the cumulative energy consumption for all node's electronics in the *ranging state*, *waiting state* and *acquisition state*. We observe that the consumed energy is directly proportional to both factors. The lowest energy consumption (30.8 mJ) corresponds to the configuration of 3 way-points and a packet size of 100 B, while the highest energy consumption (60.6 mJ) corresponds to the other extreme of the table's secondary diagonal.

The previous experiments show that the main parameters of our system are the number of way-points and the packet size. In Fig. 11, we show the energy consumption (log scale) of each module (i.e., WUR, MCU, and UWB) and its cumulative percentage contribution to the total (norm scale). Every module is shown in the ranging, waiting, and data acquisition states. Note how the energy of the ranging state only depends on the number of way-points, while the data acquisition

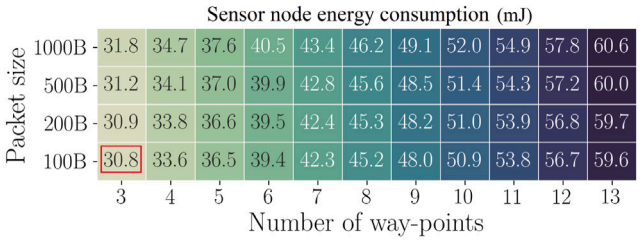

Fig. 10. Energy consumption as a function of the packet size and number of way-points.

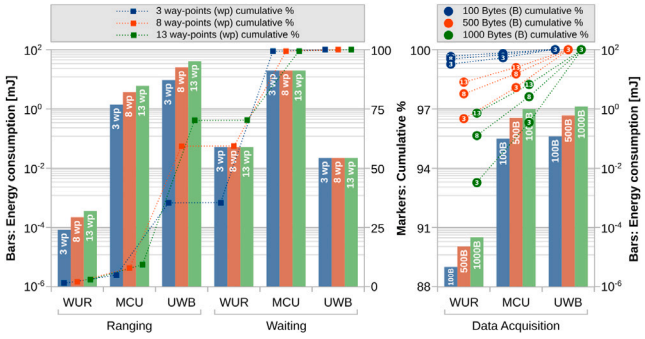

Fig. 11. The energy consumption of each electronic module during the ranging, waiting and data acquisition states.

state is affected only by the packet size, and the consumption of the waiting state is independent of both parameters. In this experiment, we keep the drone's trajectory constant in length regardless of the number of way-points, resulting in the same flight time for all configurations. We point out that the UWB is the most dominant module in terms of energy consumption in the ranging and acquisition states, while the MCU consumes more energy than the WUR or UWB in the waiting state, where the UWB is inactive. In the right subfigure, we show the energy consumption during the acquisition state and the total cumulative energy (i.e., including the energy consumed during ranging and acquisition) for three configurations of number of way-points and packet size: *i*) 3 way-points and 100 bytes, *ii*) 8 way-points and 500 bytes and *iii*) 13 way-points and 1000 bytes. We observe that the UWB consumes the most energy among the three electronic modules due to its high power consumption when active. Since in our application scenario we prioritize energy-efficiency, we choose to use three way-points, which is also a good trade-off between localization error and energy consumption as Fig. 9(b) shows.

Regarding the error in the node's localization, the UWB packet size (i.e., data acquisition phase only) does not play an important role. However, the number of bytes transmitted once the sensor node is localized and the drone has approached it is a specific parameter of the use case. For example, a sensor node equipped with a pressure sensor that takes few measurements before the drone visits it, would need to transmit a small packet. On the other side, a sensor node equipped with a camera would need to transmit much larger packets due to the large size of the images. An extensive evaluation of this specific aspect would be, therefore, out of the scope of this manuscript, where we can use the smallest possible data packet size.

5.2. Localization accuracy with a flying drone

In this section, we aim to confirm, with in-field experiments, the insights and system's properties highlighted with the data analysis from Section 5.1. Thus, we use our drone prototype on an outdoor football grass-field mission area of 40 × 40 m, situated in a semi-urban environment at 450 m above sea level with an environmental temperature

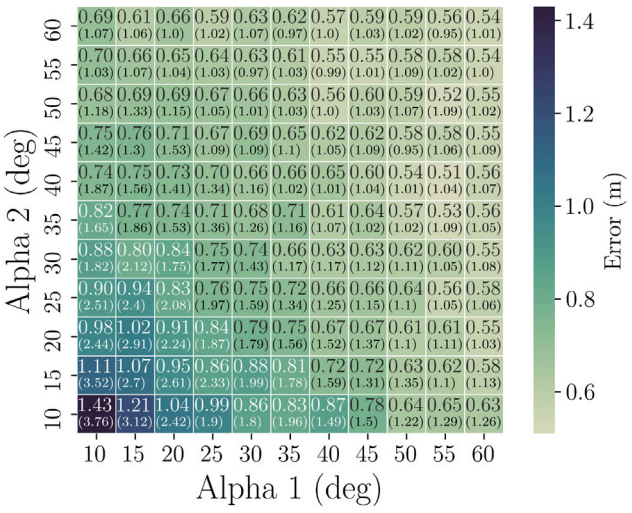

Fig. 12. Mean localization error as a function the two alpha angles — peak error in parentheses.

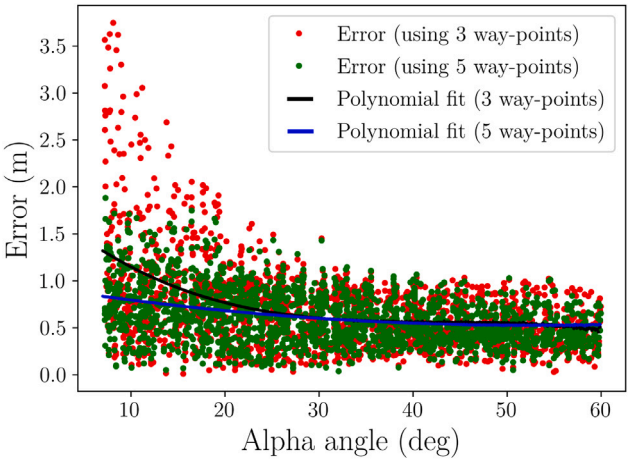

Fig. 13. Error as a function of alpha angle ($\alpha_1 \approx \alpha_2$).

of ~20 °C. We chose this environment because it is representative of the large open-space industrial facilities. However, the functionality of our system is not restricted to the operation range of UWB or WUR. In the scenario we envision, the drone's trajectory is commanded to scan the whole mission area with a resolution lower than the maximum range of the WUR. The localization mission only starts when a node receives the wake-up. In the multi-lateration algorithm, the Cartesian system's origin corresponds to the drone's take-off point, from which it flies at a constant 15 m altitude. The sensor nodes are randomly distributed in the mission area at unknown locations — by the drone. Their Cartesian coordinates are recorded to be used as ground-truth for the localization error calculation. The drone's self-localization is performed by the aboard GPS module, representing an additional source of error – root-mean-squared-error of 0.6 m – compared to the ideal scenario in Section 5.1.

In Fig. 12, we present the same exploration of the localization error as a function of the alpha angles shown in Fig. 8. This time the real-world UWB measurements are collected from our flying prototype, following the flight trajectory presented in Section 3.3. Since in this case, the real-world measurements include all the non-ideal effects of the in-field demonstration (e.g., the drone's self-localization errors), the localization accuracy drops on average of 4× compared to the synthetic data case (Fig. 8(a)), and of 52 % on average if compared to the real-world measurements acquired on the ground (Fig. 8(b)).

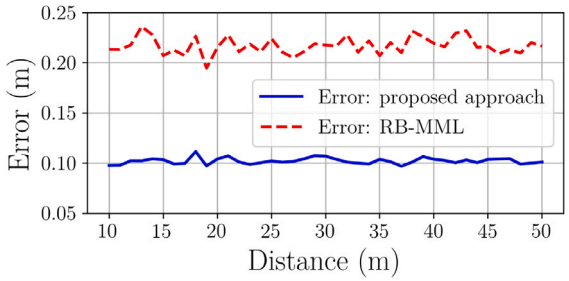

Fig. 14. Localization error as a function of distance between the drone and the sensor node.

The almost constant error on the main diagonal – and its parallels – is also confirmed in Fig. 12, showing how the error depends on the sum of the two angles. This characteristic of the error distribution allows us, without any loss of generality, to consider only one of the two alpha angles in Fig. 13. We show the localization error, and its second-order polynomial fitting, for both cases of three and five way-points — in red and green, respectively. For small alpha angles ($\alpha < 20°$), we can observe outliers that lead to errors up to 3.7 m and 1.9 m, for three and five way-points, respectively. Instead, for alpha angles of over 20° (sum of 40°), the mean error is always below 1 m. Since the additional way-points do not increase the sum of the alpha angles – i.e., the flight trajectory remains the same just increasing the number of ranging spots visited – it brings an improvement only for alpha angles lower than 20°, filtering part of the outliers out. For both considered cases, the mean of the error is around 0.6 m for angles higher than 40°, being lower bounded by the GPS position uncertainty. To ensure a certain mean error bound, a minimum alpha angle needs to be achieved, as it is guaranteed by the flight policy introduced in Section 3.3. We provide a sample dataset containing the raw data acquired with our system to facilitate the reproduction of our results.[3]

6. Discussion

We investigated the influence of the alpha angle and the number of way-points on the localization error. Furthermore, we also investigated how the localization error increases when the position of the way-points is not precisely known, being affected by the drone's self-positioning errors (i.e., GPS). This section discusses further factors that can influence the localization error and how their effect can be mitigated. Moreover, it also provides a brief overview of what is required to perform 3D sensor node localization.

Our localization scenario only focuses on LOS situations, where no obstacles are found between the drone and the sensor node. Even if this is not representative of all possible scenarios, it is still relevant for most outdoor scenarios (e.g., crop field monitoring, oceanographic sensing) and some indoor scenarios, such as greenhouses or industrial open spaces. However, our approach would still work in NLOS conditions, albeit with a decreased localization precision. For example, [35] shows that a human subject positioned right between the drone and the node during ranging introduces a bias of about 0.5 m. According to a synthetic data simulation that we performed, this would result in a localization error increased by 0.6 m for an alpha angle of 60°. To mitigate the NLOS effects, additional sensors (i.e., visual, inertial) can be used to detect and reject the outliers among the range measurements, but we leave this investigation for future works.

Another interesting exploration is the influence of the range magnitude on the localization error. We run a synthetic data simulation using a similar scenario to the one depicted in Fig. 6 where the alpha angle is fixed to 60° and the radius is swept in the range 10 m - 50 m with a step of 1 m. For every radius value, we report the localization error averaged for 300 runs of the multi-lateration algorithm, considering the same standard deviation $\sigma_r = 0.1$ m for the ranging noise as in Section 5. The results in Fig. 14 show that the localization error tends to stay constant across the whole distance range, leading to a mean error of about 0.1 m for our approach and 0.22 m for RB-MML. We further observe that our approach produces a smoother estimation which results in a standard deviation of ∼1 cm, compared to RB-MML, which is less robust to noise and whose standard deviation is ∼3 cm.

Lastly, we also investigate the influence of the altitude on the localization error by performing synthetic data experiments. To perform this investigation, we choose the locations of three way-points so that they define an equilateral triangle with the coordinates (0,0), (10,0) (5,8.7), just as in the Flight Policy. The node's position is chosen (5,-20), and it has to be determined by the localization algorithm. In this experiment, we sweep the altitude in the range 5 m–20 m with a step of 1 m. For each case, we alter the drone-node distances (for each way-point) with Gaussian noise ($\sigma = 0.1$ m), we project the measurements on the ground and estimate the position of the node using the proposed multi-lateration algorithm. We perform 300 such localization experiments for each altitude value and report the average localization error. We observe that the localization error increases linearly with the altitude for both RB-MML and our approach. In the altitude interval 5 m–20 m, the localization error is 0.48 m–0.58 m for RB-MML and 0.3 m–0.38 m for our approach. We can observe that the decrease in the altitude reduces the localization error, and for a 15 m span, the error only changes by 25%.

In this work, we address the 2D sensor node localization scenario, which is relevant for a wide range of applications as motivated in Section 1. However, the localization system can be extended to 3D in future work, which would come with additional challenges and needs. For instance, 3D localization would require an adjusted *Flight Policy* that could upper bound the 3D localization error. Furthermore, due to the need to estimate the height of the sensor node, more accurate drone altitude estimation is necessary (than the barometer). Lastly, because the range measurements in 3D are geometrically paired with spheres and not with circles as in 2D, the multi-lateration algorithm proposed in Section 3 requires a different initialization approach.

7. Conclusions & future work

This paper proposed an energy-efficient and accurate localization system that enables mobile vehicles to precisely localize wireless sensor nodes randomly deployed in the environment. The proposed approach combines the benefits of two different communication technologies, such as UWB and WUR, with a robotic platform that acts as a "ubiquitous local-host" of a WSN. Our system comprises a lightweight and accurate multi-lateration algorithm, an energy-efficient communication protocol, and a closed-loop prototype featuring our custom hardware. The proposed algorithm runs in 4 ms on a low-power MCU, bounding the localization error to 0.6 m. To enable the in-field demonstration, we developed a localization unit – that extends the functionalities aboard a COTS quadrotor – and the sensor nodes deployed in the environment. Our experimental results demonstrate how our approach can overtake SoA solutions with sub-meter real-world localization accuracy, running aboard a resource-constrained flying drone. Ultimately, the optimized communication protocol enables significant energy saving on the sensor node consuming only 31 mJ, during the whole interaction with the drone, and 3.9 µW during listening.

As future work, our localization solution can be further extended to 3D, where the sensor node's altitude is also estimated. This would involve augmenting our cost function with an additional variable z. Furthermore, the system can be further extended to work in NLOS conditions and an experimental analysis can show how the size and material of the obstacles impact the localization error. Moreover, our

[3] https://github.com/vladniculescu/UWB-WUR-Bebop-Localization.

algorithms could be ported to a nano-drone and prove their functionality in an even more computationally-constrained system, where more than 50% of the system resources are allocated for the control and estimation algorithms.

CRediT authorship contribution statement

Vlad Niculescu: Methodology, Algorithm development, Experimental evaluation, Writing – original draft preparation. **Daniele Palossi:** Methodology, Visualization, Writing. **Michele Magno:** Conceptualization, Methodology, Reviewing. **Luca Benini:** Supervision, Writing – review & editing.

Declaration of competing interest

The authors declare that they have no known competing financial interests or personal relationships that could have appeared to influence the work reported in this paper.

Acknowledgment

This work was supported in part by the Swiss National Science Foundation (SNSF), Switzerland Bridge Project "AeroSense" under Project 40B2-0_187087.

References

[1] D. Palossi, A. Marongiu, L. Benini, Ultra low-power visual odometry for nano-scale unmanned aerial vehicles, in: Design, Automation & Test in Europe Conference & Exhibition, DATE, 2017, IEEE, 2017, pp. 1647–1650.
[2] L.M. Dang, S.I. Hassan, I. Suhyeon, A. kumar Sangaiah, I. Mehmood, S. Rho, S. Seo, H. Moon, UAV based wilt detection system via convolutional neural networks, Sustain. Comput. Inf. Syst. 28 (2020) 100250.
[3] D. Palossi, F. Conti, L. Benini, An open source and open hardware deep learning-powered visual navigation engine for autonomous nano-UAVs, in: 2019 15th International Conference on Distributed Computing In Sensor Systems, DCOSS, IEEE, 2019, pp. 604–611.
[4] R.K. Goel, C.S. Yadav, S. Vishnoi, R. Rastogi, Smart agriculture–urgent need of the day in developing countries, Sustain. Comput. Inf. Syst. 30 (2021) 100512.
[5] A. Rajput, V.B. Kumaravelu, Scalable and sustainable wireless sensor networks for agricultural application of internet of things using fuzzy c-means algorithm, Sustain. Comput. Inf. Syst. 22 (2019) 62–74.
[6] M. van Geest, B. Tekinerdogan, C. Catal, Design of a reference architecture for developing smart warehouses in industry 4.0, Comput. Ind. 124 (2021) 103343.
[7] A. Kaushik, D. Lobiyal, Localization in mobile wireless sensor networks using drones, Trans. Emerg. Telecommun. Technol. (2021) e4213.
[8] M. Farooq-I-Azam, Q. Ni, E.A. Ansari, Intelligent energy efficient localization using variable range beacons in industrial wireless sensor networks, IEEE Trans. Ind. Inf. 12 (6) (2016) 2206–2216.
[9] C. Zhan, Y. Zeng, R. Zhang, Energy-efficient data collection in UAV enabled wireless sensor network, IEEE Wirel. Commun. Lett. 7 (3) (2017) 328–331.
[10] D. Popescu, F. Stoican, G. Stamatescu, O. Chenaru, L. Ichim, A survey of collaborative UAV–WSN systems for efficient monitoring, Sensors 19 (21) (2019) 4690.
[11] B. Etzlinger, A. Ganhör, J. Karoliny, R. Hüttner, A. Springer, Wsn implementation of cooperative localization, in: 2020 IEEE MTT-S International Conference on Microwaves for Intelligent Mobility, ICMIM, IEEE, 2020, pp. 1–4.
[12] A. Gomez, M. Magno, M.F. Lagadec, L. Benini, Precise, energy-efficient data acquisition architecture for monitoring radioactivity using self-sustainable wireless sensor nodes, IEEE Sens. J. 18 (1) (2017) 459–469.
[13] A. Gilchrist, Industry 4.0: The Industrial Internet Of Things, Springer, 2016.
[14] S. Narayana, R.V. Prasad, V. Rao, L. Mottola, T.V. Prabhakar, Hummingbird: energy efficient GPS receiver for small satellites, in: Proceedings of the 26th Annual International Conference on Mobile Computing and Networking, 2020, pp. 1–13.
[15] K. Minne, N. Macoir, J. Rossey, Q. Van den Brande, S. Lemey, J. Hoebeke, E. De Poorter, Experimental evaluation of UWB indoor positioning for indoor track cycling, Sensors 19 (9) (2019) 2041.
[16] M. Magno, V. Jelicic, B. Srbinovski, V. Bilas, E. Popovici, L. Benini, Design, implementation, and performance evaluation of a flexible low-latency nanowatt wake-up radio receiver, IEEE Trans. Ind. Inf. 12 (2) (2016) 633–644.
[17] L. Perilli, E.F. Scarselli, R. La Rosa, R. Canegallo, Wake-up radio impact in self-sustainability of sensor and actuator wireless nodes in smart home applications, in: 2018 Ninth International Green and Sustainable Computing Conference, IGSC, IEEE, 2018, pp. 1–7.
[18] F.B. Sorbelli, S.K. Das, C.M. Pinotti, S. Silvestri, On the accuracy of localizing terrestrial objects using drones, in: 2018 IEEE International Conference on Communications, ICC, IEEE, 2018, pp. 1–7.
[19] H. Sallouha, M.M. Azari, S. Pollin, Energy-constrained UAV trajectory design for ground node localization, in: 2018 IEEE Global Communications Conference, GLOBECOM, IEEE, 2018, pp. 1–7.
[20] S. Sadowski, P. Spachos, Rssi-based indoor localization with the internet of things, IEEE Access 6 (2018) 30149–30161.
[21] J.H. An, L. Choi, Inverse fingerprinting: server side indoor localization with bluetooth low energy, in: 2016 IEEE 27th Annual International Symposium on Personal, Indoor, and Mobile Radio Communications, PIMRC, IEEE, 2016, pp. 1–6.
[22] M. Larsson, V. Larsson, K. Astrom, M. Oskarsson, Optimal trilateration is an eigenvalue problem, in: ICASSP 2019-2019 IEEE International Conference on Acoustics, Speech and Signal Processing, ICASSP, IEEE, 2019, pp. 5586–5590.
[23] D. Niculescu, B. Nath, Ad hoc positioning system (APS) using AOA, in: IEEE INFOCOM 2003. Twenty-Second Annual Joint Conference of the IEEE Computer and Communications Societies (IEEE Cat. No. 03CH37428), Vol. 3, IEEE, 2003, pp. 1734–1743.
[24] B.J. Silva, G.P. Hancke, Ranging error mitigation for through-the-wall non-line-of-sight conditions, IEEE Trans. Ind. Inf. (2020).
[25] S. Bottigliero, D. Milanesio, M. Saccani, R. Maggiora, A low-cost indoor real-time locating system based on TDOA estimation of UWB pulse sequences, IEEE Trans. Instrum. Meas. 70 (2021) 1–11.
[26] T.-K. Le, K. Ho, Joint source and sensor localization by angles of arrival, IEEE Trans. Signal Process. 68 (2020) 6521–6534.
[27] V. Cantón Paterna, A. Calveras Auge, J. Paradells Aspas, M.A. Perez Bullones, A bluetooth low energy indoor positioning system with channel diversity, weighted trilateration and kalman filtering, Sensors 17 (12) (2017) 2927.
[28] A. Vashist, D.R. Bhanushali, R. Relyea, C. Hochgraf, A. Ganguly, P.S. Manoj, R. Ptucha, A. Kwasinski, M.E. Kuhl, Indoor wireless localization using consumer-grade 60 GHz equipment with machine learning for intelligent material handling, in: 2020 IEEE International Conference on Consumer Electronics, ICCE, IEEE, 2020, pp. 1–6.
[29] A.E. Varjovi, S. Babaie, Green internet of things (gIoT): Vision, applications and research challenges, Sustain. Comput. Inf. Syst. 28 (2020) 100448.
[30] J. Xu, J. He, Y. Zhang, F. Xu, F. Cai, A distance-based maximum likelihood estimation method for sensor localization in wireless sensor networks, Int. J. Distributed Sens. Netw. 12 (4) (2016) 2080536.
[31] V. Niculescu, M. Magno, D. Palossi, L. Benini, An energy-efficient localization system for imprecisely positioned sensor nodes with flying UAVs, in: International Conference on Industrial Informatics, IEEE, 2020, pp. 188–193.
[32] J. Li, X. Yue, J. Chen, F. Deng, A novel robust trilateration method applied to ultra-wide bandwidth location systems, Sensors 17 (4) (2017) 795.
[33] A. Lesage-Landry, J.A. Taylor, I. Shames, Second-order online nonconvex optimization, IEEE Trans. Autom. Control (2020).
[34] W. Zhao, A. Goudar, J. Panerati, A.P. Schoellig, Learning-based bias correction for ultra-wideband localization of resource-constrained mobile robots, 2020, arXiv preprint arXiv:2003.09371.
[35] C. Lian Sang, M. Adams, T. Hörmann, M. Hesse, M. Porrmann, U. Rückert, Numerical and experimental evaluation of error estimation for two-way ranging methods, Sensors 19 (3) (2019) 616.